SUPPLEMENTARY MATERIAL

Contents

1. Sources of Ion Current Modulation in Nanopore Experiments

Understanding the ion current through the nanopore is essential in properly analyzing enzyme kinetics with SPRNT. There are several potential sources of ion current modulation in nanopore systems:

(1) Enzyme / DNA motion
(2) Access resistance changes caused by the enzyme resting close to MspA
(3) Fluctuations caused by contamination of ions other than K^+ and Cl^-
(4) Interactions between the DNA bases and MspA

Our goal is to decouple current changes caused by enzyme activity from the other sources of current modulation.

In the Hel308 ion current traces, we observed that many ion current steps (both [ATP]-dependent and [ATP]-independent) tended to have short-lived decreases in ion current amplitude (5-50 ms) that could not be associated with any Hel308 ion current state, before returning to the previous ion current step (Fig. s1a). We call such ion current states 'flickers'. Because flickers occurred as only downwards spikes in the current trace, it is also unlikely that flickers are caused by DNA motion through the pore, as we would expect this to lead to both current increases and decreases (27). To test if flickers were caused by ion contamination or interactions between the DNA bases and MspA, we performed an experiment in which we placed both phi29 DNA polymerase (29) and Hel308 into the reaction volume. Flickers were observed only in the translocation events with Hel308, suggesting that Hel308 is required for flickering, and thus flickers are not an effect of the ion contamination or MspA-DNA interactions. We thus attribute flickering behavior to a transient access resistance caused by interactions between Hel308 and MspA. We conclude that the flickers are not caused by enzymatic activity. Therefore, when examining dwell times we must include flickers together with the associated step.

We analyzed the data by performing sequence alignment of the current amplitudes for each event to a reference consensus (27,28). Flickers tended to be aligned to an incorrect step, so we corrected each alignment manually using a custom-made GUI.

2. Conversion of Ion Current to DNA Position

As an enzyme walks along a DNA strand and feeds it into the MspA pore, we observe a series of discrete ion current steps (Fig. s1a). Previously, we found that these ion current steps observed during nanopore sequencing are a discrete sampling of a smooth underlying curve of ion current versus DNA position(27). This smooth curve is what one would observe if they were to smoothly feed DNA through the pore and plot the measured ion current vs. the DNA position within the pore. Using alignment algorithms similar to Needleman-Wunch alignment(28,37,38) this smooth curve can also be used as a direct mapping from measured ion current to DNA position within the pore.

To make this conversion, one needs to know the underlying smooth current vs. position curve for the particular sequence of DNA used. Previously, we found that the Hel308 helicase steps in two approximately half-nucleotide steps on ssDNA (27) ([ATP]-dependent step forwards to ATP-independent:0.55 ± 0.03 nt and [ATP]-independent forwards to [ATP]-dependent: 0.45 ± 0.03 nt). In this manuscript, we approximate this smooth underlying curve with a spline curve determined from the consensus of current values observed while Hel308 helicase steps DNA through the pore. Consensus DNA positions are spaced according to our previous measurement (0, 0.45 nt, 1.0 nt, 1.45 nt, 2.0 nt, ...; fig s1b). A given raw SPRNT current measurement can then be converted from ion current to position via the following steps:

(1) Find and extract average ion current values for steps in the data (Fig. s1a). This is described in detail in (26).
(2) Align extracted ion current step means to the previously measured consensus. For alignment we use a dynamic programming algorithm similar to Needleman-Wunch alignment (28,37,38). For a detailed explanation of alignment of nanopore currents, see Laszlo 2016, Appendix C (26). Average ion current steps for 20 example events have been aligned to the consensus in Figure s1b.
(3) Use the alignment from (2) to match each ion current datapoint from the ion current measurement to the corresponding DNA position. Bulk alignment of ion current steps to the consensus provides initial context that allows individual ion current datapoints to be matched to the underlying smooth curve. Because the measured currents are not unique to a particular position (i.e. multiple positions along the DNA result in similar or identical ion current measurements), bulk alignment of current steps allows us to determine where on the spline to look for a corresponding ion current/position pair. Matching is done via a T-test comparison of each measured current value to all spline current values that lie within 3 nt of the bulk-aligned position. The spline has some uncertainty in it because there is variability in the observed currents from measurement to measurement (see aligned levels in Fig s1b), this uncertainty is used as the standard deviation, σ, in the T-test. For each measured ion current datapoint, the T-test yields a liklihood of match for each current/position pair of the spline (within 3 nt of the bulk alignment). It sometimes occurs that there are two or three best possible current matches. This happens when the measured enzyme step is close to a peak or trough in the underlying smooth curve, thus a measured current point can match spline current values to the left and right of the peak/trough. We resolve this ambiguity by using our knowledge of the overall alignment to assign a prior probability to the T-test output. We thus multiply the position likelihood scores by an assigned prior probability that is a normalized Gaussian of width $\sigma = 0.7$ nt, centered at the position of the alignment. Figure s1 panels c, d, and e show in schematic form how ion current is transduced into position using the smooth current vs. position curve.

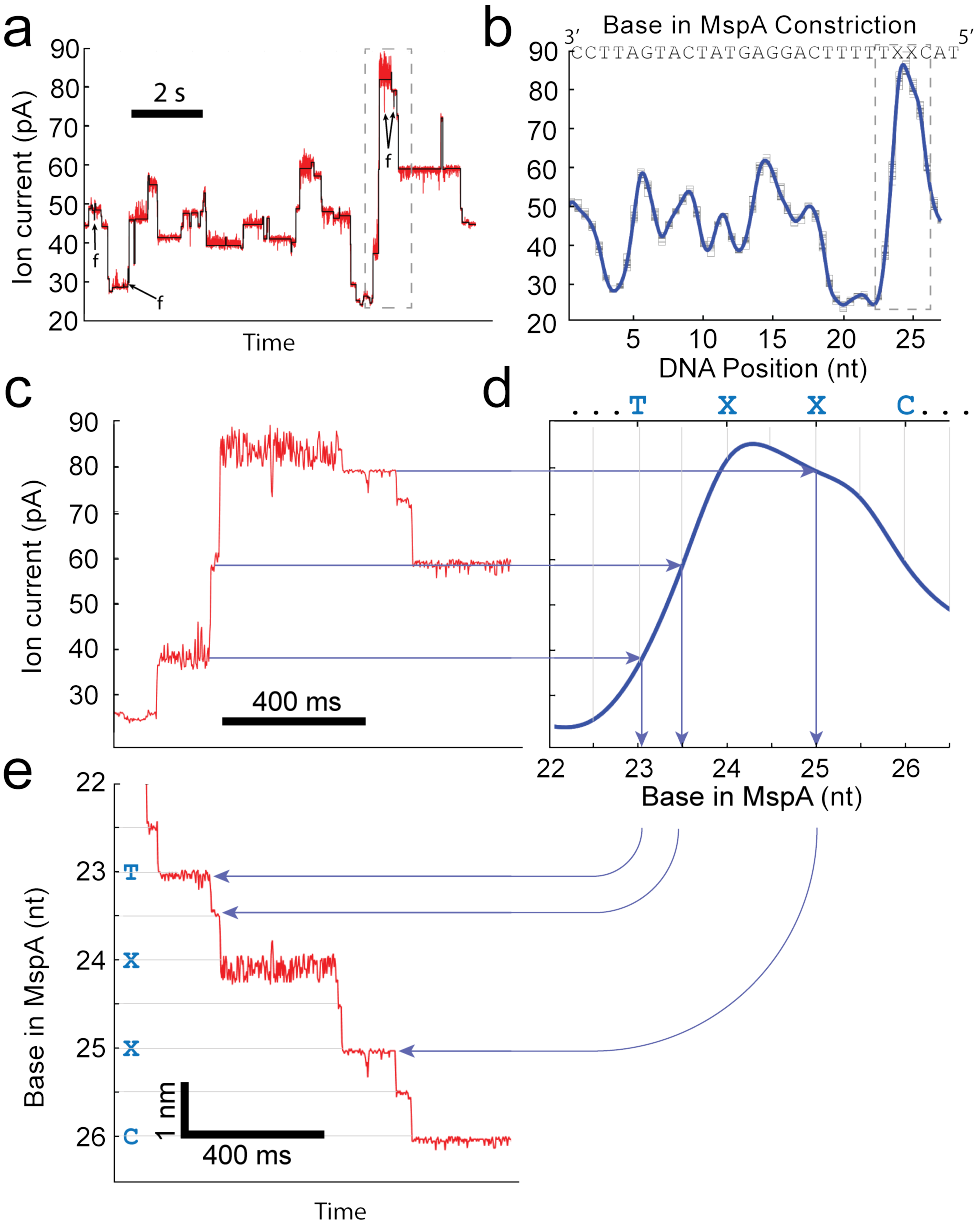

FIGURE S1. Conversion of ion current to DNA position. (a) Raw data trace of ion current versus time for the same event shown in figure 1c. Flickers are indicated by an 'f' (b) Smooth ion current versus DNA position curve, constructed by averaging together many reads like those in (a)(27). The DNA sequence in the MspA constriction is displayed above, with 'X' indicating an abasic site. (c-e) Each data point in the ion current versus time trace (c) is mapped to the underlying smooth curve (d) as indicated by the arrows, thereby determining the DNA position versus time (e).

Experiment	$[ATP](\mu M)$	$[ADP](\mu M)$	$Voltage(mV)$	$Temperature(^{\circ}C)$	N_{events}
ATPt	10	0	180	22	34*
ATPt,ADPi,Voltage II	50	0	180	22	47*
ATPt	100	0	180	22	38
ATPt	250	0	180	22	59*
ATPt,Temperature,Voltage I	500	0	180	22	36*
ATPt	1000	0	180	22	99*
ATPt	2000	0	180	22	35
ATPt	3000	0	180	22	57*
ADPi	50	10	180	22	22
ADPi	50	25	180	22	44
ADPi	50	50	180	22	30
ADPi	50	100	180	22	32
ADPi, Ratio [ATP]:[ADP]=1:4	50	200	180	22	27
Ratio [ATP]:[ADP]=1:4	300	1200	180	22	15
Ratio [ATP]:[ADP]=1:4	500	2000	180	22	33
Ratio [ATP]:[ADP]=1:4	700	2800	180	22	34
Voltage I	500	0	140	22	37
Voltage I	500	0	160	22	27
Voltage I	500	0	200	22	41
Voltage I	500	0	220	22	37
Voltage I	500	0	240	22	55
Voltage I	500	0	260	22	37
Voltage I	500	0	280	22	35
Voltage II	50	0	140	22	34
Voltage II	50	0	220	22	45
Voltage II	50	0	260	22	26
Temperature	500	0	180	28	17
Temperature	500	0	180	34	65
Temperature	500	0	180	45	28
Ratio [ATP]:[ADP]=1:2	10	20	180	37	39
Ratio [ATP]:[ADP]=1:2	50	100	180	37	30
Ratio [ATP]:[ADP]=1:2	100	200	180	37	22
Ratio [ATP]:[ADP]=1:2	250	500	180	37	40
Ratio [ATP]:[ADP]=1:2	500	1000	180	37	24
Ratio [ATP]:[ADP]=1:2	750	1500	180	37	48
Ratio [ATP]:[ADP]=1:2	1500	3000	180	37	27

TABLE S1. Experimental conditions and number of Hel308 events. The experiments tags are as follows. ATPt refers to experiments in which only the ATP concentration was varied. An asterisk indicates some data was used in a previous publication (27). ADPi refers to experiments in which the ADP concentration was varied at $[ATP] = 50\ \mu M$. Voltage I and Voltage II refer to experiments in which the voltage was varied while maintaining $[ATP] = 500\ \mu M$ and $[ATP] = 50\ \mu M$, respectively. Ratio refers to experiments in which we maintained a constant ratio of $[ATP] : [ADP] = 1 : 4$ or $[ATP] : [ADP] = 1 : 2$. Temp refers to experiments in which the temperature was varied at $[ATP] = 500\ \mu M$. In total $N = 1357$ single-molecule data traces were obtained for this study.

3. The Master Equation

To analyze different kinetic models at the single-molecule level we use the master equation formalism (41), which describes the way that probability flows between different enzyme states. The master equation can be used to answer questions such as: what is the average dwell time of an observable state as a function of the substrate concentration? What is the probability that the motor enzyme steps backwards? What is the distribution of dwell times for $f|f$ steps? Consider the toy model shown in figure s2, a four state model consisting of chemical states A, B_1, B_2, and C which transition between one another. Transitions between A and B_1, and B_2 and C result in a change in ion current signal, while transitions between B_1 and B_2 are hidden. Assume that at time 0 (i.e. the start of a new DNA position measurement) the enzyme is in state B_1. The rate of change of the probability that the enzyme occupies state B_1 is obtained by summing the rate of probability flow into state B_1, and subtracting the rate of probability flow out of state B_1:

$$\frac{dp_{B_1}}{dt} = p_{B_2} \cdot k_{-1} - p_{B_1} \cdot (k_{-0} + k_1) \tag{s1}$$

Equations of this form can be written for states, A, B_2 and C as well. Then we note that these are a linear system of differential equations, which allows us to write the matrix equation:

$$\frac{d\vec{p}}{dt} = \frac{d}{dt}\begin{bmatrix} p_A \\ p_{B_1} \\ p_{B_2} \\ dp_C \end{bmatrix} = M \cdot \vec{p}(t) = \begin{bmatrix} 0 & k_{-0} & 0 & 0 \\ 0 & -k_{-0} - k_1 & k_{-1} & 0 \\ 0 & k_1 & -k_{-1} - k_2 & 0 \\ 0 & 0 & k_2 & 0 \end{bmatrix} \cdot \begin{bmatrix} p_A \\ p_{B_1} \\ p_{B_2} \\ p_C \end{bmatrix}. \tag{s2}$$

equation S2 is called the 'master equation' for this system. The entries of $\vec{p}(t)$ are the probabilities that the individual states are occupied at time t and M is the called 'connection matrix'. Diagonal entries of M are outflow rates from a given state, while off diagonal entries M_{ij} are the rate of probability flow from state j into state i. The columns of M must always sum to 0 to conserve probability. In this example we start in state B_1, therefore the initial conditions for equation s2 are:

$$\vec{p}(t=0) = \begin{bmatrix} 0 \\ 1 \\ 0 \\ 0 \end{bmatrix}. \tag{s3}$$

The master equation together with the initial conditions completely specify the system. The solution to equation s2 is easily written in terms of the eigenvalues of the connection matrix:

$$\vec{p}(t) = \Sigma_i c_i \cdot \vec{\xi_i} \cdot exp(\lambda_i \cdot t), \tag{s4}$$

where λ_i and $\vec{\xi_i}$ are the eigenvalues and eigenvectors of M, and c_i are the coefficients of integration. The c_i can be solved according to the initial conditions:

$$\vec{c} = V^{-1} \cdot \vec{p}(t=0) \tag{s5}$$

where V is a matrix whose columns are the $\vec{\xi_i}$. In principle, we have fully solved the problem, however for complex kinetic models with many states and parameters the eigenvalues cannot be analytically solved. Thus using equation s4 can be difficult. In the remainder of this supplement we will use several different techniques to analyze solutions to the master equation, such as the steady-state approximation, numerical solutions, direct integration and laplace transform.

It is important to discuss here how this formalism connects to experimental data. For example, when displaying the kinetic model in figure s2 why did we not include the transition $A \xrightarrow{k_0} B_1$ and $C \xrightarrow{k_{-2}} B_2$? These terms are certainly important, but not relevant to the experimental question we are asking: what is that probability distribution of dwell times for the enzyme to go between observable states given that we begin in state B_1? This is an example of the 'first-passage time' problem. If we were to include $A \xrightarrow{k_0} B_1$ in this diagram and the master equation, then we would be including information from multiple different observable

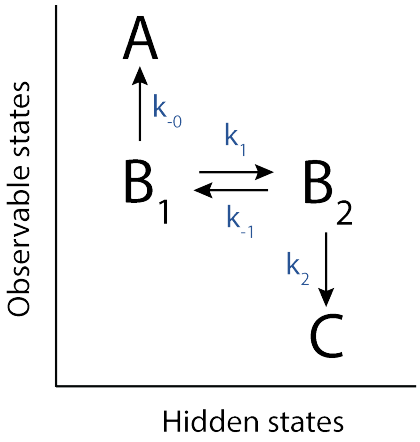

FIGURE S2. A simple kinetic model to illustrate the master equation.

states into our model, which complicates interpretation of the data. The term $A \overset{k_0}{\rightarrow} B_1$ would be included in discussing the master equation for a different observable state.

$[ATP](\mu M)$	10	50	100	250	500	1000	2000	3000
N^i_{total}	424	1807	576	1159	493	1658	541	944
N^i_{ave}	18	75	24	48	21	69	23	39

TABLE S2. The total number of measured f|f steps for the [ATP]-dependent step (N^i_{total}) and average number of measurements for each step (N^i_{ave}) at the given ATP concentration.

4. Statistical Analysis of Michaelis-Menten Parameters for [ATP]-dependent f|f Steps

We tested whether the variation among measured Michaelis-Menten parameters (figure s3a) for $f|f$ [ATP]-dependent steps $V_{f|f}$ and $K_{f|f}$, as defined by the Michaelis equation could have been produced by statistical fluctuations. We asked the following statistical question: what is the probability of observing the joint distribution of experimentally measured $V_{f|f}$ and $K_{f|f}$, given that $V_{f|f}$ and $K_{f|f}$ do not depend on DNA position (the null-hypothesis). We generated data for the null-hypothesis by placing all of the data for each [ATP]-dependent step (all half-integer DNA positions) at a given [ATP] into a single bin. The number of data points in a single concentration i is N^i_{total}. Let the average number of times a given DNA position is measured at a concentration i be N^i_{ave} (table s2). For each concentration we drew N^i_{ave} measurements of the dwell time at random from the N^i_{total} measurements. We took the mean and standard deviation of the mean of each of these bins, and performed a weighted fit to the Michaelis-Menten equation, extracting the values of $V_{f|f}$ and $K_{f|f}$. These parameters represent 1 Monte Carlo sample in our null hypothesis. We repeated this process 10^5 times, which is justified because $10^5 \ll Choose(N^i_{total}, N^i_{ave})$ for each experiment, ensuring that each Monte Carlo sample is independent. Figure s3b shows the joint distribution of $K_{f|f}$ and $V_{f|f}$ for both the Monte Carlo samples and the measured values (blue and red, with solid and dashed black lines representing the error ellipses, respectively). It is clear that many of the experimental data points could not have been produced randomly at confidence $p < 10^5$. As such, we reject the null hypothesis that the measured distribution of $K_{f|f}$ and $V_{f|f}$ could have been randomly produced at confidence $p \ll 10^5$.

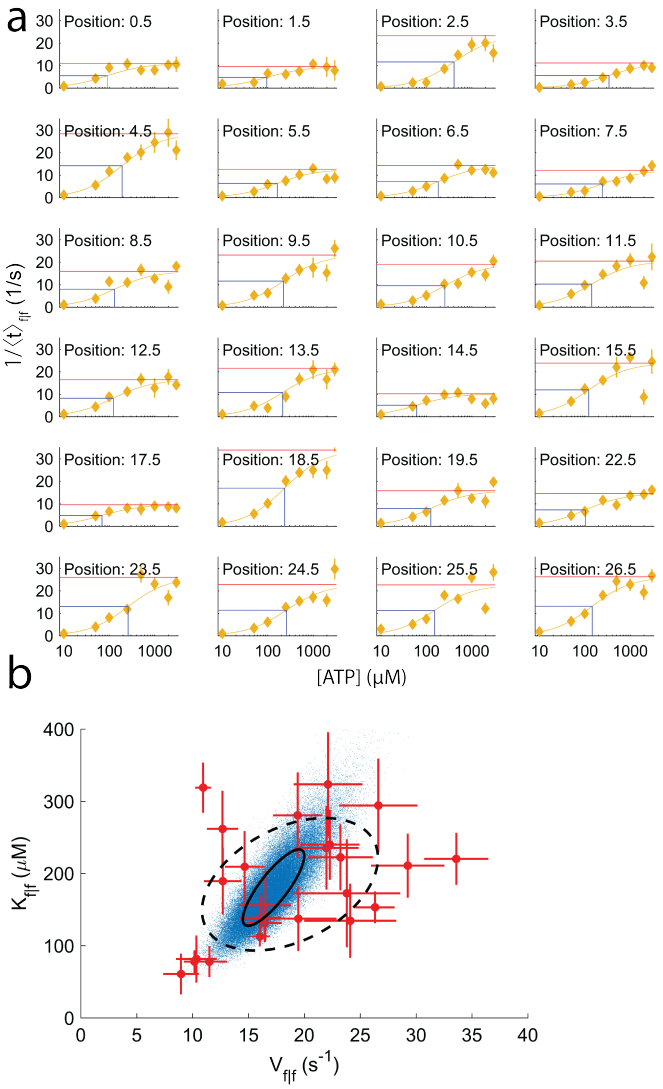

FIGURE S3. (a) The rate of [ATP]-dependent f|f steps versus [ATP] at several DNA positions (positions 16.5 20.5 and 21.5 are ommitted due to degenerate ion current signals). The best fit of the Michaelis-Menten equation to the data is plotted on top (yellow line). The red line indicates the best fit value of the maximum rate of reaction ($V_{f|f}$). The horizontal blue line corresponds to $V_{f|f}/2$, with the vertical blue line showing the position of $K_{f|f}$. (b) The distribution of Michaelis parameters for [ATP]-dependent steps (red). Crosses are the 1 S.E.M. measured error. Each blue dot is a Monte Carlo simulation, generated by taking the data from each step, drawing randomly and fitting a Michaelis Menten equation to the resulting mean values. The solid and dashed black curves are error ellipses for the Monte Carlo simulation and the measured data, respectively.

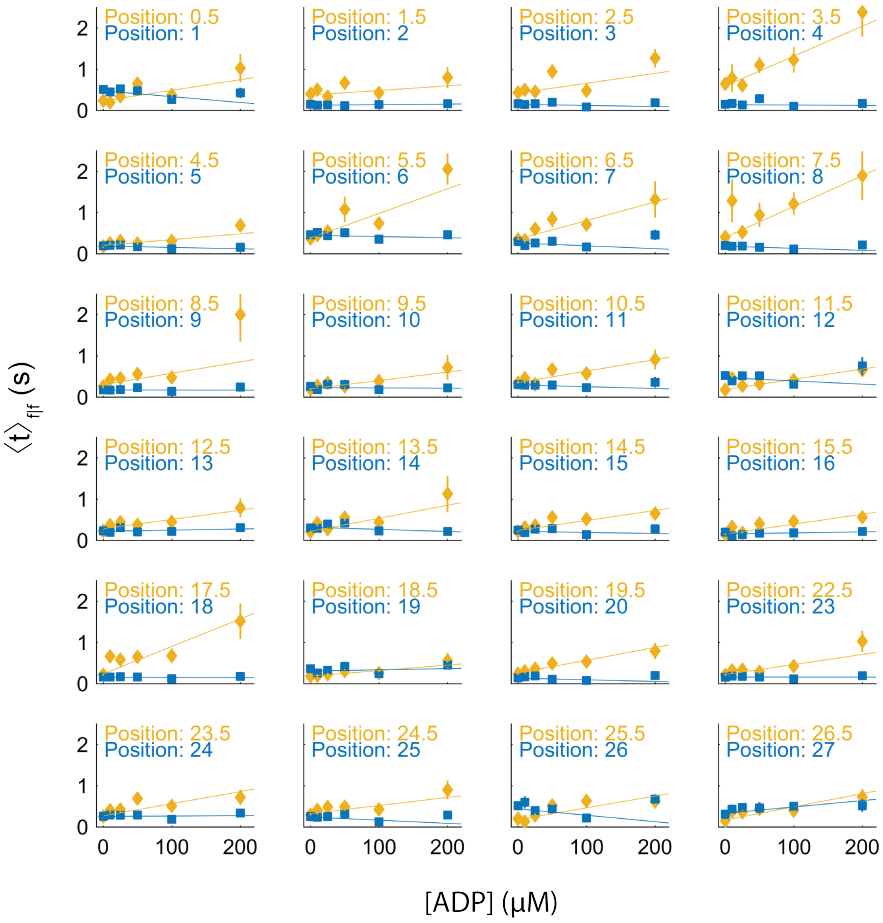

FIGURE S4. The average dwell time of f|f [ATP]-dependent steps (yellow, half-integer DNA positions) and [ATP]-independent steps (blue, integer DNA positions) as a function of the [ADP]. The best linear fits are plotted on top. The average dwell time of the [ATP]-dependent step increases linearly with [ADP], while the average dwell time of the [ATP]-independent step does not depend on [ADP].

5. Comparing f|f and f|b [ATP]-dependent steps

To compare f|f to f|b [ATP]-dependent steps, we analyzed only those DNA positions in which the following [ATP]-independent step went backwards sufficiently often to accumulate enough statistics to analyze the ATP dependence of f|b [ATP]-dependent steps. Figure s5a shows the rate of reaction for f|f and f|b [ATP]-dependent steps. Each of these curves are nearly identical, and produce similar values of V and K when fit to the Michaelis-Menten equation. The expressions for V and K for f|f and f|b steps from Model 1 are:

$$V_{f|f} = k_2 \cdot \frac{k_D}{k_2 + k_D}, V_{f|b} = k_2 \tag{s6}$$

$$K_{f|f} = \frac{k_{-T} + k_2}{k_T} \cdot \frac{k_D}{k_2 + k_D}, K_{f|b} = \frac{k_{-T}}{k_T} \tag{s7}$$

where the subscript indicates the step type (figure 6a, for derivations see Discussion s6, s10). If we have that $k_D \gg k_2$ then $V_{f|f} = V_{f|b}$, and if we additionally have that $k_{-T} \gg k_2$ then $K_{f|f} = K_{f|b}$. Evaluating the model parameters for the [ATP]-dependent step confirms this to true in most cases (on average $k_{-T} \approx 30\ s^{-1}$, $k_D \approx 170\ s^{-1}$, $k_2 \approx 17\ s^{-1}$, for all DNA positions see table s7). In some cases k_{-T} is similar in value to k_2, but the errors on the fit value of K are fairly large ($\approx 20 - 40\%$ for individual steps), so it may be difficult to distinguish differences between $K_{f|f}$ and $K_{f|b}$.

Figure s5b shows the dwell time distributions for the DNA positions (2.5, 7.5, 9.5 and 24.5) at subsaturating ($[ATP] = 50\ \mu M$, top row) and saturating ($[ATP] = 1\ mM,\ 2\ mM,\ 3\ mM$, bottom row) [ATP]. We used the 2-sample KS test to evaluate the similarity of each of the [ATP]-dependent f|f and f|b dwell time distributions (Fig. s5), and found that each pair of histograms was statistically indistinguishable ($p > 0.05$ for each pair of histograms). These results can be explained by one the following two arguments:

(1) If the preceding b|f [ATP]-independent step is an off-pathway backwards step resulting from an unproductive forwards step, then we would expect that the initial conditions do not modify the kinetics, because the initial conditions are actually unmodified.
(2) If the preceding b|f [ATP]-independent step is an on-pathway backwards step, then because the ATP and ADP off rates (k_{-T} and k_D) are large when compared with k_2, thus we would expect that f|f and f|b steps both effectively start in the free enzyme state (unbound Hel308), which would lead to similar kinetics.

It is impossible to distinguish between which of these cases is actually occurring due to the similarity of b|f and f|f [ATP]-independent steps (Fig s5) and the values of the Model 1 parameters (Table s7).

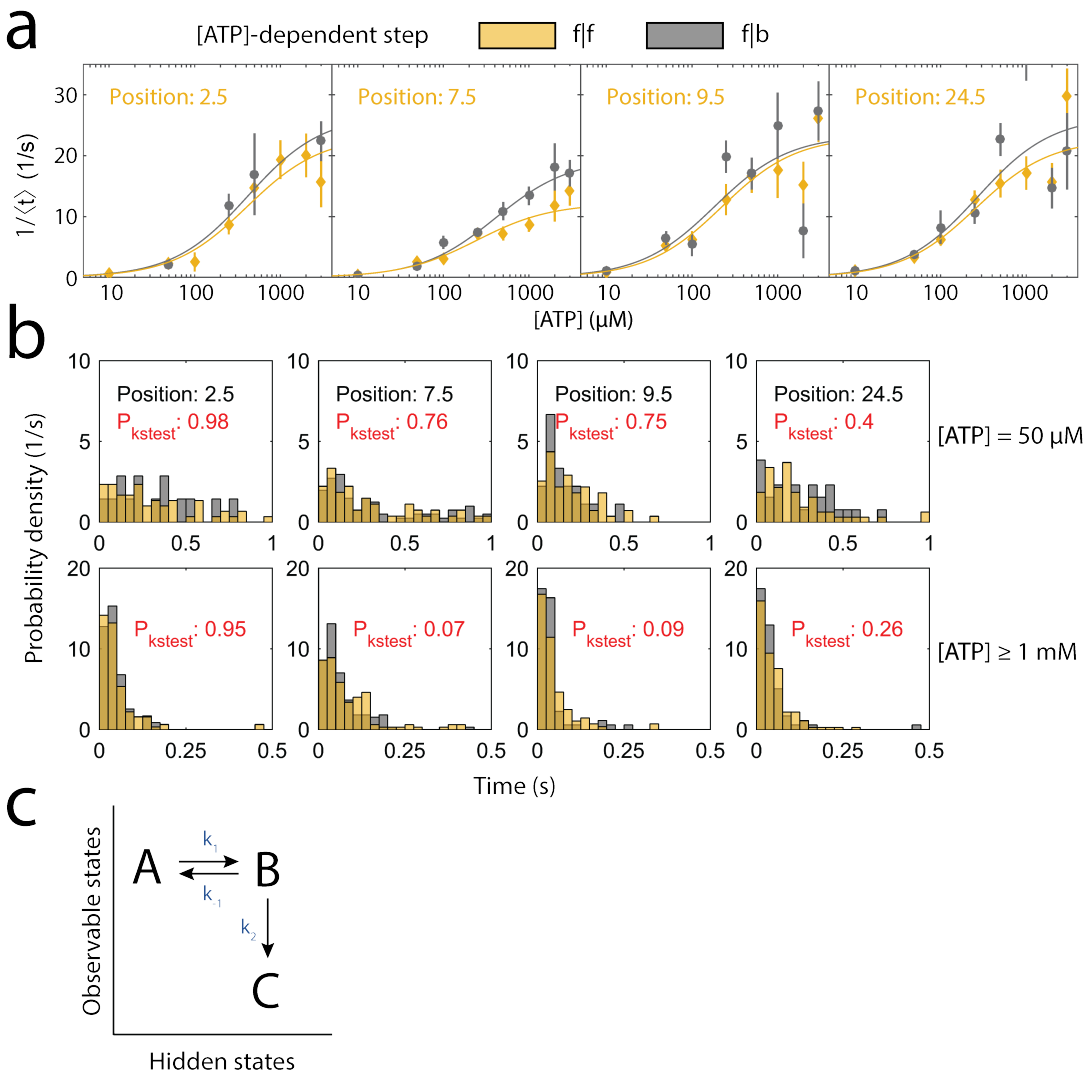

FIGURE S5. Comparing f|f and f|b [ATP]-dependent steps. (a) The rate of reaction for f|f (yellow) and f|b (grey) [ATP] dependent steps vs. [ATP] for several different DNA positions. Best fit to the Michaelis-Menten equation is plotted on top. The x-axis is logarithmic. (b) (Top) Dwell time distributions of the [ATP]-dependent step at given positions along the DNA at [ATP]=50μM for f|f steps (yellow) and f|b steps (grey). The p-value for the two-sample KS test is displayed in red, indicating that the histograms are statistically indistinguishable. (c) A kinetic model to analyze f|b steps.

6. Derivation of a Dwell time Distribution Function for General f|b Steps

To examine modified initial conditions in our experiments, we considered a simple kinetic model shown in figure s5. The connection matrix for this model is:

$$M = \begin{bmatrix} -k_1 & k_{-1} & 0 \\ k_1 & -k_2 - k_{-1} & 0 \\ 0 & k_2 & 0 \end{bmatrix}. \tag{s8}$$

We solve the master equation (eq. s2) subject to the initial conditions that at time 0 we start in state B:

$$\vec{p}(t=0) = \begin{bmatrix} 0 \\ 1 \\ 0 \end{bmatrix}. \tag{s9}$$

After some algebra, the dwell time distribution is shown to be:

$$\frac{dq}{dt}(t) = k_2 p_2(t) = \eta \cdot \lambda_+ e^{-\lambda_+ \cdot t} + (1-\eta) \cdot \lambda_- e^{-\lambda_- \cdot t} \tag{s10}$$

where $\eta = k_2 \cdot \frac{1+\frac{k_1}{\lambda_+}}{2|D|}$, D^2 is the discriminant of the characteristic equation, $Det(I\lambda - M) = 0$, and $-\lambda_\pm$ are the non-zero eigenvalues of M. By averaging over equation s10 for Model 1 (Fig. 6A) in the absence of ADP we can show:

$$\langle t \rangle = \int_0^\infty t \cdot \frac{dq}{dt} \cdot dt = \frac{K_{f|b} + [ATP]}{V_{f|b} \cdot [ATP]}, \tag{s11}$$

where $V_{f|b} = k_2$ and $K_{f|b} = k_{-T}/k_T$. In the limit that $k_3 \gg k_2$ and $k_{-T} \gg k_2$ we have that $K_{f|f} \approx K_{f|b}$ and $V_{f|f} \approx V_{f|b}$. Evaluating the parameters for this model (discussion s11) suggests that this is the case, which could potentially explain the similarity of the curves in figure s5.

7. Analysis of Probability of Backwards Steps

We define the probability of a backwards step for a DNA position j as:

$$p_{back,j} = \frac{N_{b|f,j}}{N_{b|f,j} + N_{f|f,j}}, \tag{s12}$$

where $N_{f|f,j}$ and $N_{b|f,j}$ are the observed number of forwards and backwards steps following forwards steps for step j. For figures 4 and 6 in the main text we average over all DNA positions so that

$$p_{back,condition} = \frac{\Sigma_j N_{b|f,j}}{\Sigma_j N_{f|f,j} + N_{b|f,j}}. \tag{s13}$$

The error on this measurement is calculated using the binomial distribution:

$$\delta p_{back} = \sqrt{\frac{p_{back} \cdot (1 - p_{back})}{N_{f|f} + N_{b|f}}}. \tag{s14}$$

Figure s6 shows the probability of a backstep for the [ATP]-independent step at different DNA positions, averaged over each ATP and ADP titration experiment.

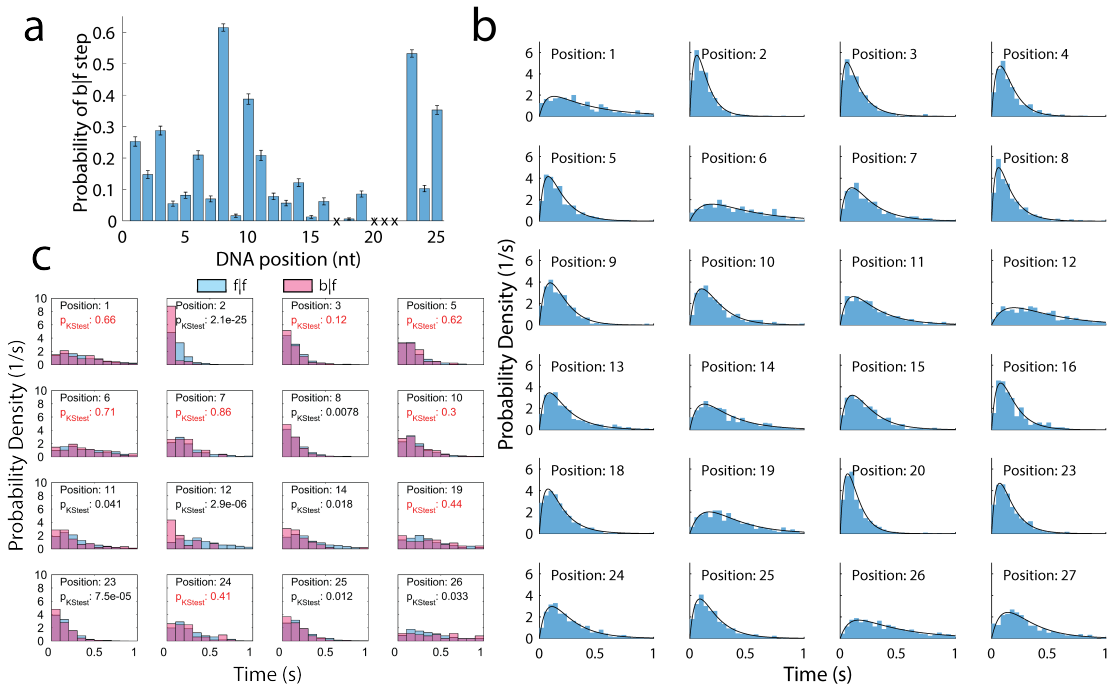

FIGURE S6. (a) Probability of a b|f step versus DNA position for the [ATP]-independent step. An 'x' indicates the the measurement could not be made due to adjacent ion current levels being too similar. (b) The distribution of dwell times for [ATP]-independent f|f steps (light blue), constructed by taking data from each ATP and ADP titration experiment. The best-fit curve to equation s17 is plotted on top in black. (c) Dwell time distributions for f|f (blue) and b|f (pink) [ATP]-independent steps with $N \geq 50$ counts of the b|f step. The p-value for the two-sample KS test are displayed. In many instances the distributions are statistically indistinguishable (Those steps with $p > 0.05$, indicated in red).

8. Analysis of f|f and f|b [ATP]-independent Dwell time Distributions Using the AIC

We analyzed the dwell time distributions of [ATP]-independent steps using the corrected Akaike Information criterion (AIC (39)) to analyze f|f and f|b steps. Information (i.e. the predictive power of the model) is lost when data is used to approximate a 'true' underlying distribution function, and when overly complex models are applied to describe the data. The AIC chooses a model by minimizing the information loss of candidate models. The AIC is given by:

$$AIC = \frac{k \cdot (k+1)}{N-k-2} + k - log(L(\hat{\theta}|t)), \tag{s15}$$

where k is the number of parameters in the model, N is the number of measured data points, L is the likelihood function, and $\hat{\theta}$ is the maximum likelihood estimator for the parameters of the model. The model with the smallest value of the AIC is the one which minimizes the information loss of the data out of the candidate models. We analyzed the following four classes of distribution function:

$$\frac{dp}{dt}(t|a) = a \cdot e^{-a \cdot t} \tag{s16}$$

$$\frac{dp}{dt}(t|a,b) = \frac{a \cdot b}{a-b} \cdot (e^{-b \cdot t} - e^{-a \cdot t}) \tag{s17}$$

$$\frac{dp}{dt}(t|a,b,c) = a \cdot b \cdot c \left[\frac{e^{-a \cdot t}}{(c-a)(b-a)} + \frac{e^{-b \cdot t}}{(c-b)(a-b)} + \frac{e^{-c \cdot t}}{(a-c)(b-c)} \right] \tag{s18}$$

$$\frac{dp}{dt}(t|a,b,c) = a \cdot b \cdot e^{-b \cdot t} + (1-a) \cdot c \cdot e^{-c \cdot t} \tag{s19}$$

Equations s16-s18 are the convolutions of 1, 2 and 3 exponentials, respectively, as would be expected for a Markov chain model (40). Equation s19 is a possible model for f|b steps (see section 6).

Because the dwell time distribution changes along DNA position for f|f and f|b steps (Fig. 5), we calculate the maximum likelihood estimators for each DNA position (i) and each class of distribution function (j), $\hat{\theta}_{ij}$, and sum the AICs for each DNA position together to compute the total information loss, and compare the models. That is:

$$AIC_{total,model\ j} = \Sigma_{i=1}^{N_{steps}} AIC_{ij}. \tag{s20}$$

The values for the $AIC_{total,modelj}$ are displayed in table s3. From this table we conclude that, out of the four candidate distribution functions, the information loss is minimized for f|f steps by the convolution of two exponetial distributions, suggesting that there are two rate-limiting steps in the f|f [ATP]-independent step. In contrast, for f|b steps the information loss is minimized by the mixed-exponential model s19.

Model	k	$AIC_{f\|f}$	$AIC_{f\|b}$
single exponential (eq s16)	1	-3617.0	-281.4
2 convolved exponentials (eq s17)	2	-4264.4	-278.3
3 convolved exponentials (eq s18)	3	-4263.5	-267.3
mixed exponentials (eq s19)	3	-3694.2	-297.7

TABLE S3. The AIC values for the [ATP]-independent f|f and f|b steps for several candidate distribution functions. The value which minimizes the AIC minimizes the information loss by assuming the given model. In total $N_{f|f} = 10052$ and $N_{f|b} = 365$ dwell time measurements of the $f|f$ and $f|b$ steps were used, respectively.

DNA position (nt)	$a_{f\|f}$ (s^{-1}, eq. s17)	$b_{f\|f}$ (s^{-1}, eq. s17)	$a_{f\|b}$ (eq. s19)	$b_{f\|b}$ (s^{-1}, eq. s19)	$c_{f\|b}$ (s^{-1}, eq. s19)
1	2.4 ± 0.2	35 ± 16	-	-	-
2	8.2 ± 0.5	43 ± 7	-	-	-
3	7.8 ± 0.4	38 ± 7	-	-	-
4	7.1 ± 0.4	28 ± 4	1	12 ± 4	-
5	5.8 ± 0.3	32 ± 6	-	-	-
6	2.3 ± 0.1	13 ± 3	0.15 ± 0.14	1.3 ± 0.8	6.3 ± 1.4
7	4.2 ± 0.2	24 ± 4	-	-	-
8	6.5 ± 0.3	45 ± 8	-	-	-
9	7.2 ± 0.6	18 ± 3	-	-	-
10	4.1 ± 0.2	27 ± 5	1	6.8 ± 1.4	-
11	4.0 ± 0.3	19 ± 4	-	-	-
12	2.5 ± 0.2	11 ± 2	0.44 ± 0.19	2.0 ± 0.8	12 ± 5
13	4.3 ± 0.2	32 ± 6	-	-	-
14	3.6 ± 0.2	17 ± 3	-	-	-
15	5.8 ± 0.5	16 ± 3	0.72 ± 0.15	6.3 ± 1.5	68 ± 45
16	7.5 ± 0.6	20 ± 4	-	-	-
18	6.9 ± 0.5	27 ± 6	-	-	-
19	3.0 ± 0.2	13 ± 2	1	11 ± 3	-
23	8.2 ± 0.5	24 ± 4	0.09 ± 0.08	1.1 ± 0.9	16 ± 5
24	5.3 ± 0.4	14 ± 3	1	11 ± 5	-
25	5.7 ± 0.3	23 ± 4	0.47 ± 0.26	4.3 ± 1.8	22 ± 13
26	2.0 ± 0.1	19 ± 4	0.65 ± 0.07	2.2 ± 0.4	55 ± 15

TABLE S4. Fit parameters for [ATP]-independent steps. The rate parameters for fits to equation s17 for f|f steps are displayed in columns 2 and 3, while the parameters for fits to equations s19 for f|b steps are shown in columns 4, 5, and 6. If there were < 20 counts of the f|b step then those columns were left blank. For certain DNA positions fits to eq. s19 the parameter a came out as exactly 1 or 0, meaning that for those DNA positions a single exponential is a better model to describe the data, and therefore only the single exponential fit eq. s16 is reported, with the final column left blank.

9. Voltage and Temperature Variation

The force dependence of the dwell time $\langle t \rangle(F)$ in motor enzymes is typically described by the following formula (44):

$$\langle t \rangle(F) = A \cdot exp(\frac{\Delta E + F \cdot \delta x}{RT}), \tag{s21}$$

where A is a prefactor with units of time, ΔE is the activation energy of the reaction, F is the force applied to the DNA against the direction of motion of the motor, δx is the characteristic enzyme step size, and RT is the temperature in units of energy. In SPRNT we assume that the electrostatic force on the DNA is proportional to the applied voltage V:

$$\langle t \rangle(V) = A \cdot exp(\frac{\Delta E + \alpha \cdot V}{RT}), \tag{s22}$$

where α has units of charge. At constant temperature we can write:

$$\langle t \rangle(V) = A' \cdot exp(\beta \cdot V). \tag{s23}$$

Figures s7a and s7b show the average dwell time of f|f steps for both [ATP]-dependent and [ATP]-independent steps, averaged over DNA position, plotted against voltage at $[ATP] = 500\ \mu M$ and $[ATP] = 50\ \mu M$, respectively. The results of fitting equation s23 to the data are displayed in table s5. In each case we find

$\beta \approx 0$, suggesting that the kinetics are independent of voltage in the range of voltages applied. In figure s7b the average duration appears to decrease slightly with increasing voltage, however, the fit is highly skewed by the data point at $V = 140\ mV$. In addition, because Hel308 is pulling the DNA out of the pore against the force, we would expect that the average dwell time increases with increasing force. We therefore suggest that the decrease in dwell time with voltage in figures7b is not statistically significant.

Setting $\alpha = 0$ in equation s22 gives:

$$\langle t \rangle = A \cdot exp(\frac{\Delta E}{RT}). \tag{s24}$$

Figure s7c shows the average dwell time of f|f [ATP]-dependent and [ATP]-independent steps versus the inverse temperature of the solution. Fits to equation s24 yield $\Delta E_{[ATP]-dep} = 60 \pm 11\ kJ \cdot mol^{-1}$ and $\Delta E_{[ATP]-indep} = 77 \pm 15\ kJ \cdot mol^{-1}$. Becasue there are multiple chemical substates within both the [ATP]-dependent and [ATP]-independent pathways, and because we average over DNA position in constructing these curves, these numbers represent approximately the average activation energy of the rate-limiting step for each observable step type.

State	$[ATP]$ (μM)	β (mV^{-1})
[ATP]-dep	500	0.001 ± 0.002
[ATP]-indep	500	0.001 ± 0.001
[ATP]-dep	50	-0.002 ± 0.005
[ATP]-indep	50	0.0001 ± 0.004

TABLE S5. Best fit value of β to equation s23 for the curves shown in figure s7.

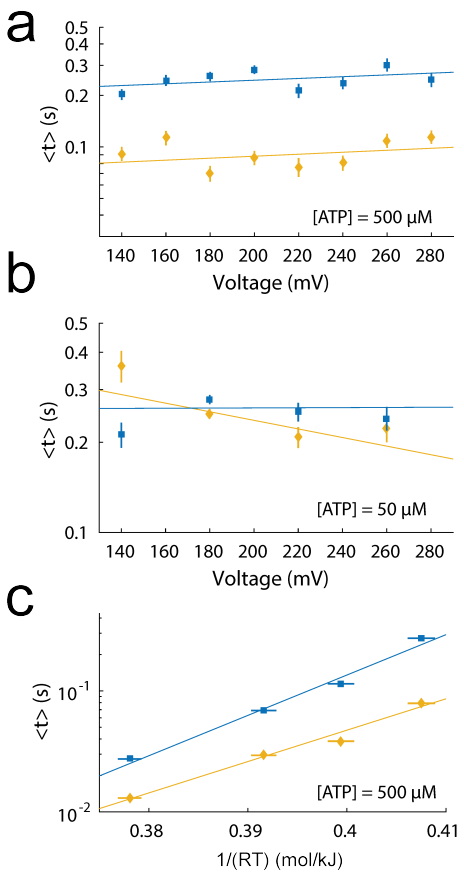

FIGURE S7. (a) The average dwell time of [ATP]-dependent (yellow) and [ATP]-independent (blue) steps averaged over DNA position vs. voltage at $[ATP] = 500\ \mu M$. The y-axis is logarithmic. Best fits to equation s23 are plotted on top. The fit parameters are displayed in table s5. (b) The average dwell time of [ATP]-dependent (yellow) and [ATP]-independent (blue) steps averaged over DNA position vs. voltage at $[ATP] = 50\ \mu M$. The y-axis is logarithmic. Best fits to equation s23 are plotted on top. The fit parameters are displayed in table s5. (c) The average dwell time taken over all [ATP]-dependent (yellow) and [ATP]-independent (blue) steps averaged over DNA position vs. inverse temperature at $[ATP] = 500\ \mu M$. The y-axis is logarithmic. Best fits to equation s22 are plotted on top. All error bars are S.E.M. The error bars in temperature in (c) represent day-to-day and experiment-to-experiment fluctuations in temperature.

10. Calculation of Average Dwell Time of f|f [ATP]-dependent Steps Using the Steady-state Approximation

The goal of this section is to calculate the average dwell time of f|f [ATP]-dependent steps for both Model 1 and Model 2 as a function of [ATP] and [ADP]. Because there are four states in Model 1, the eigenvalues of the connection matrix come from a cubic polynomial, and solutions are difficult to calculate. Similarly, for Model 2 there are five states, which requires solving a quartic polynomial to obtain the eigenvalues. Thus, we seek to rewrite this problem to make use of the steady-state approximation (32), which can be used to determine average dwell times by solving a linear system of equations. First we note that none of the processes which determine the dwell time of the [ATP]-independent step can affect the average dwell time of the [ATP]-dependent step, so we compress the rate constants $k_{\pm H}$, $k_{\pm P}$, and k_1 into a single rate parameter Ω. Restricting ourselves to f|f steps means we can ignore k_{-2}. We use the fact that for the [ATP]-dependent step $p_{b|f} \ll 1$ to conclude that $k_{-1} \ll k_D$ (Model 1) or $k_{-1} \ll k_T[ATP]$ (Model 2), so we can ignore k_{-1} as well. Figure s8 summarizes each of these observations into a single kinetic path for Model 1. In this form, we can use the steady-state approximation so that:

$$M \cdot \vec{p}_{ave} = \vec{0}, \tag{s25}$$

where M is the connection and $\vec{p}_{ave}$ is the average probability that a given state is occupied. The normalization condition is:

$$\Sigma_i \; p_{ave,i} = 1, \tag{s26}$$

where i indexes the entries of $\vec{p}_{ave}$. The connection matrix for Model 1 in this approximation is:

$$M_{Model\ 1} = \begin{bmatrix} -k_D & k_{-D}[ADP] & 0 & \Omega \\ k_D & -k_{-D}[ADP] - k_T[ATP] & k_{-T} & 0 \\ 0 & k_T[ATP] & -k_{-T} - k_2 & 0 \\ 0 & 0 & k_2 & -\Omega \end{bmatrix} \tag{s27}$$

Equations s26 and s27 are used to solve for $p_{ave,i}$. Following Keller (32), the total reaction rate for Model 1 is the average probability that the ATP bound state of Hel308 is occupied multiplied by the transition rate:

$$r_{total,Model\ 1} = \frac{1}{\langle t \rangle_{total,Model\ 1}} = k_2 \cdot p_{ave,Hel308 \cdot ATP}, \tag{s28}$$

We are interested in the rate of just the $f|f$ [ATP]-dependent step. The average total time to progress through the entire pathway is the sum of the time to go through the [ATP]-dependent step plus the time to go through the [ATP]-independent step:

$$\langle t \rangle_{total,Model\ 1} = \langle t \rangle_{[ATP]_d \to [ATP]_i} + \langle t \rangle_{[ATP]_i \to [ATP]_d} = \langle t \rangle_{[ATP]_d \to [ATP]_i} + \frac{1}{\Omega} \tag{s29}$$

The transition rate for [ATP]-dependent steps can be solved by rearranging equation s29.

$$rate_{[ATP]_d \to [ATP]_i} = \frac{1}{\langle t \rangle_{[ATP]_d \to [ATP]_i}} = (\langle t \rangle_{total} - \frac{1}{\Omega})^{-1} \tag{s30}$$

Plugging the results of s26, s27 and s28 into s30 for Model 1 yields:

$$rate_{Model\ 1} = \frac{V \cdot [ATP]}{K + [ATP] + d \cdot [ADP]} \tag{s31}$$

Applying an identical calculation to Model 2 gives:

$$rate_{Model\ 2} = \frac{V' \cdot [ATP]}{K' + [ATP] + d' \cdot [ADP] + e \cdot [ATP] \cdot [ADP]} \tag{s32}$$

where $K = \frac{k_{-T}+k_2}{k_T} \cdot \frac{k_D}{k_2+k_D}$, $V = \frac{k_2 \cdot k_D}{k_2+k_D}$, $d = K \cdot \frac{k_{-D}}{k_D}$, $V' = \frac{k_T k_2 k_D k_H}{D}$, $K' = \frac{k_{-T}k_2k_D + k_{-T}k_2k_{-H} + k_2k_Dk_H}{D}$, $d' = \frac{k_{-D}k_{-T}k_{-H}}{D}$, $e = \frac{k_{-D}k_T(k_H+k_{-H})}{D}$, with $D = k_Tk_2k_D + k_Tk_2k_{-H} + k_Tk_2k_H + k_Tk_Dk_H$. Equations s31 and s32 are independent of Ω, as they must be. These expressions differ qualitatively only by the existence of the term $e \cdot [ATP] \cdot [ADP]$ that couples the ATP and ADP concentrations in equation s32.

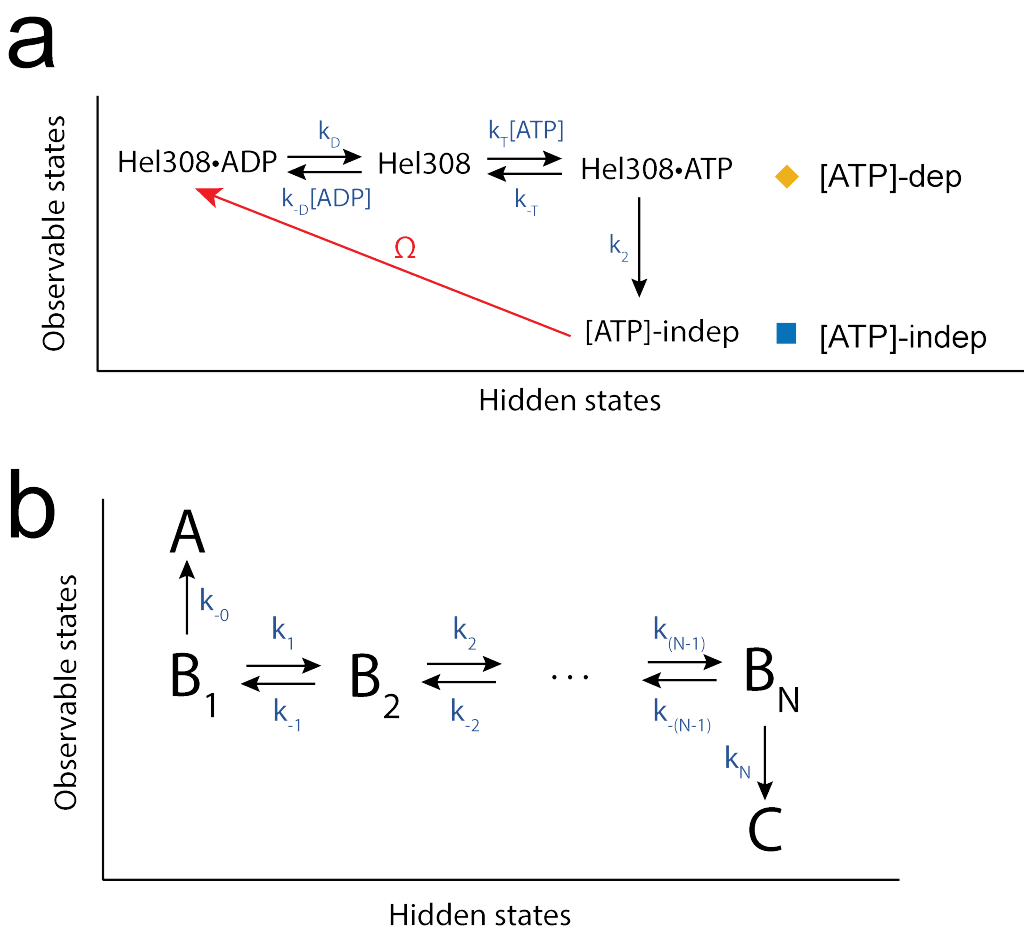

FIGURE S8. (a) The kinetic model from main text figure 6a, reduced to a form that allows easy application of the steady-state approximation.(b) A hypothetical model to illustrate how to calculate the backstep probability in a chain Markov model.

11. Derivation of the Probability of a b|f Step for [ATP]-dependent Steps in Model 1 and Model 2

Because SPRNT gives us access to both forwards and backwards steps, we sought to derive a general formula for the probability of a backstep in terms of the underlying rate constants of a given kinetic model. Consider the hypothetical kinetic model shown in figure s8b. Assume that at time 0 the enzyme is in the state B_1. In the first passage time problem, the only states that can be occupied at time ∞ are A and C, corresponding to a backwards step and a forwards step, respectively. The probability of a backstep is thus:

$$p_{back} = \lim_{t\to\infty} p_A(t). \tag{s33}$$

As done previously, we solve the equation $\frac{d\vec{p}}{dt}(t) = M\cdot\vec{p}(t)$, however in this case we use the Laplace transform method. We define $\vec{p}(s) = \mathcal{L}(\vec{p}(t))$ to be the laplace transform of $\vec{p}(t)$. The solution in transform space is easily shown to be:

$$\vec{p}(s) = (sI - M)^{-1}\cdot\vec{p}(t=0), \tag{s34}$$

where I is the identity matrix. The inverse transformation is done by the Bromwich integral(43):

$$p_j(t) = \Sigma_{i=1}^{N_{poles}} Res_{s=s_i}[p_j(s)\cdot e^{s\cdot t}] \tag{s35}$$

where j indexes the entries of $\vec{p}$. $Res_{s=s_i}[p_j(s)e^{s\cdot t}]$ is the residue evaluated at the poles s_i of $p_j(s)$, and s is taken as a complex variable. The backstep probability can be written using equations s33 and s35 as:

$$p_{back} = \lim_{t\to\infty} \Sigma_{i=1}^{N_{poles}} Res_{s=s_i}[p_A(s)\cdot e^{s\cdot t}]. \tag{s36}$$

This sum is over a finite number of poles, so we interchange the limit and residue expressions, and because $p_A(s)$ is not a function of time:

$$p_{back} = \Sigma_{i=1}^{N_{poles}} Res_{s=s_i}[p_A(s)\cdot \lim_{t\to\infty} e^{s_i\cdot t}]. \tag{s37}$$

Note that we have explicitly evaluated the residue in the exponential term $e^{s_i\cdot t}$. Next we use the fact that the poles of $p_i(s)$ are eigenvalues of the matrix M, which in the first-passage time problem have the property that $s_i \leq 0$. The limit as $t\to\infty$ vanishes for all negative eigenvalues, collapsing the sum and leaving us with the simple expression:

$$p_{back} = Res_{s=0}[p_A(s)], \tag{s38}$$

where $P_A(s)$ is determined from equation s34. If the pole at $s=0$ is first order then this expression reduces to:

$$p_{back} = \lim_{s\to 0} s\cdot p_A(s). \tag{s39}$$

Other expressions have been derived for the backstep probability (30,31), but to our knowledge, the form of equation s39 has not been derived. This expression is simple to apply, because both the matrix inversion and residues of rational functions are easy to evaluate. Applying equation s39 to Model 1 and Model 2 yields:

$$p_{back,Model\ 1} = \frac{k_{-1}k_{-D}(k_2+k_{-T})[ADP] + k_{-1}k_2k_T[ATP]}{k_{-1}k_{-D}(k_2+k_{-T})[ADP] + (k_{-1}+k_D)k_2k_T[ATP]}, \tag{s40}$$

$$p_{back,Model\ 2} = \frac{k_{-1}(k_2k_Dk_H + k_{-T}k_2k_D + k_2k_{-H}k_{-T} + k_{-D}k_{-H}k_{-T}[ADP])}{k_{-1}(k_2k_Dk_H + k_{-T}k_2k_D + k_2k_{-H}k_{-T} + k_{-D}k_{-H}k_{-T}[ADP]) + k_2k_Dk_Hk_T[ATP]}. \tag{s41}$$

To apply equation s39 to Model 1 with the additional diffusion term, we simply need to note that in this model we have $p_{back} = \lim_{t\to\infty}(p_{Hel308^*\cdot ADP} + p_{Hel308^*})$, giving:

(s42)
$$p_{back,Model\ 1+diffusion} = \frac{2k_{dif}(k_{-1}+k_D)(k_2+k_{-T}) + k_{-1}k_{-D}(k_2+k_{-T})[ADP] + k_{-1}k_2k_T[ATP]}{2k_{dif}(k_{-1}+k_D)(k_2+k_{-T}) + k_{-1}k_{-D}(k_2+k_{-T})[ADP] + (k_{-1}+k_D)k_2k_T[ATP]}.$$

First, we note that in the limiting case of $[ADP] \to 0$ in equation s40, $p_{back,Model\ 1} \to \frac{k_{-1}}{k_{-1}+k_D}$, as must be the case for a simple branched pathway. In order to do fitting with these models, we rearrange expressions s40-s42 into more accessible forms using the forms of V,K,d,V',K' and d' from equations s31-s32:

(s43)
$$p_{back,Model\ 1} = \frac{d[ADP] + \frac{V}{k_D}[ATP]}{d[ADP] + \frac{V}{k_D}[ATP](1+\frac{k_D}{k_{-1}})}$$

(s44)
$$p_{back,Model\ 2} = \frac{K' + d'[ADP]}{K' + d'[ADP] + \frac{V'}{k_{-1}}[ATP]}$$

(s45)
$$p_{back,Model\ 1+diffusion} = \frac{2\frac{k_{dif}}{k_D}(1+\frac{k_D}{k_{-1}})K + d[ADP] + \frac{V}{k_D}[ATP]}{2\frac{k_{dif}}{k_D}(1+\frac{k_D}{k_{-1}})K + d[ADP] + \frac{V}{k_D}[ATP](1+\frac{k_D}{k_{-1}})}.$$

We have managed to write s40-s42 in terms of the same proportionality constant (d or d') with which the average dwell time depends on $[ADP]$ at fixed $[ATP]$. It is important to specify at least one of these parameters when doing fits to equations s43-s45, because without a parameter to set the scale, there will always be some degeneracy, due to the fact that p_{back} will be unchanged by scaling the concentrations and rate constants by a constant factor. Ultimately, for model selection, we are interested in the quality of the fit given a certain value of d, so we use $d = 0.003$, obtained from averaging over each DNA position in table s6. Fits to equations s43-s45 to the data p_{back} vs. $[ATP]$ and $[ADP]$ for all experiments are displayed in figure s9c. Of the three models considered here, Model 1 together with the diffusion term (black line) best fits the data.

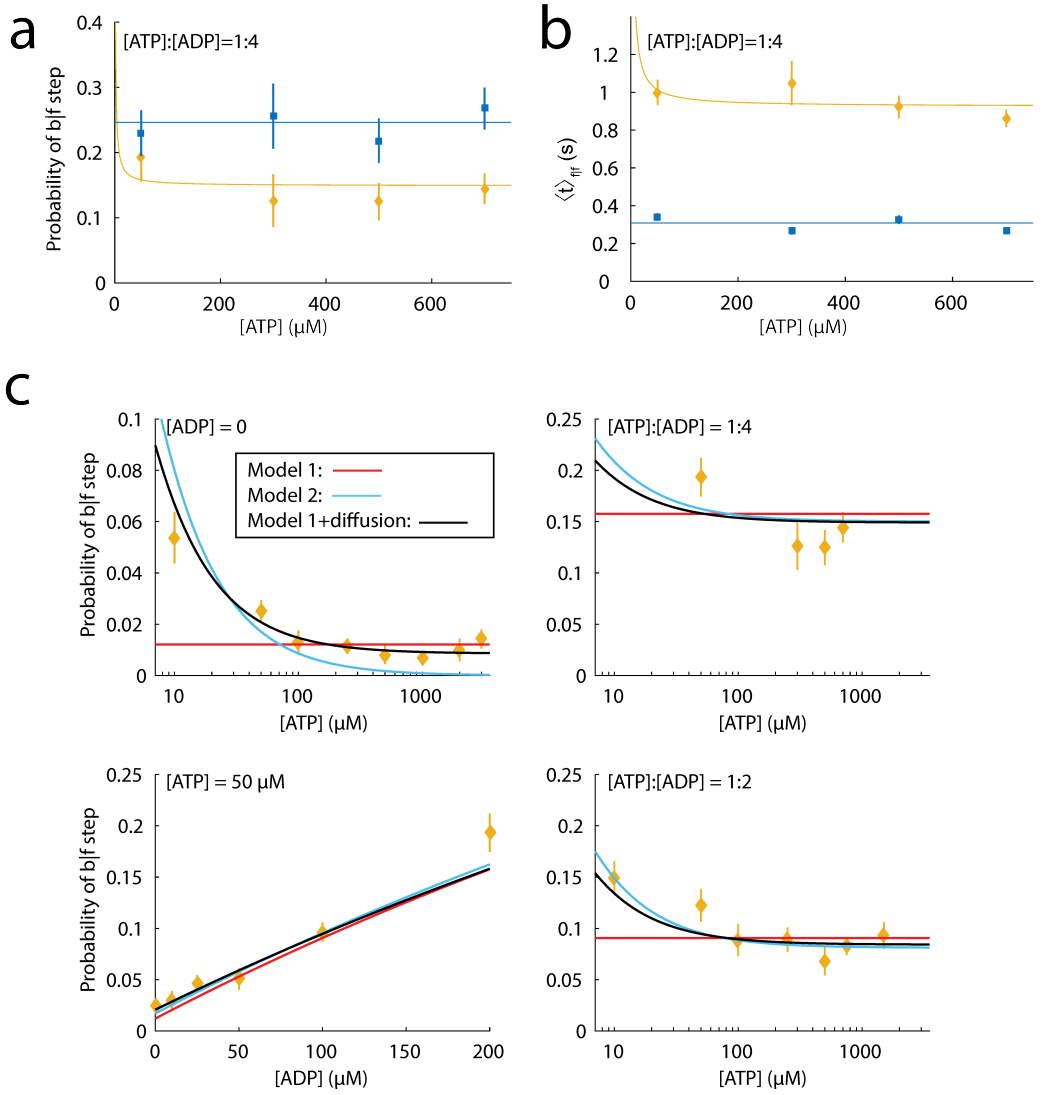

FIGURE S9. (a) Probability of a backstep for the [ATP]-dependent (yellow) and [ATP]-independent (blue) steps averaged over DNA position vs. [ATP] at fixed ratio [ATP]:[ADP] = 1:4. Weighted averages to the data are plotted on top. (b) Average dwell time of f|f [ATP]-dependent (yellow) and [ATP]-independent (blue) step averaged over DNA position vs. [ATP] at fixed ratio [ATP]:[ADP] = 1:4. Best fit to main text equation 3 is plotted on the [ATP]-dependent step, yielding $e^* \approx 0$, in line with Model 1. The weighted average (blue) is plotted on the [ATP]-independent step. (c) Probability of a $b|f$ step in several different experiments: (top left) $[ATP]$ varied, $[ADP] = 0$. (bottom left) $[ATP] = 50\mu M$, $[ADP]$ varied. (top right) $[ATP]$ and $[ADP]$ varied at fixed $[ATP] : [ADP] = 1{:}4$. (bottom right) $[ATP]$ and $[ADP]$ varied at fixed $[ATP] : [ADP] = 1{:}2$. Red, blue and black lines are simultaneous fits to the data in each of the panels shown for Model 1 (red, eq. s43, $\chi^2/\nu = 3.0$), Model 2 (blue, eq. s44, $\chi^2/\nu = 2.9$) and Model 1 with diffusion (black, eq. s45, $\chi^2/\nu = 1.0$), respectively.

12. Estimation of Kinetic Parameters for [ATP]-dependent Steps

To gain further insight into Hel308 kinetics, we calculated the relevant kinetic parameters for the [ATP]-dependent step using likelihood maximization. From Model 1 (Fig 6a) and the ATP and ADP titration experiments we estimated the 5 parameters that determine the progression of [ATP]-dependent f|f steps $(k_{\pm T}, k_2, k_{\pm D})$ using maximum likelihood methods. Here we assume that $k_{-1} \ll k_D$, an assumption that is justified by the low probability of a backstep for [ATP]-dependent steps in the absence of ADP ($p_{back} < 0.01$ for most DNA positions, so any errors made under this assumption are small compared to the errors on $V_{f|f}$ and $K_{f|f}$). The probability distribution of dwell times for a kinetic model is determined by numerically solving the master equation with connection matrix:

$$M = \begin{bmatrix} -k_D & k_{-D} \cdot [ADP] & 0 & 0 \\ k_D & -k_{-D} \cdot [ADP] - k_T \cdot [ATP] & k_{-T} & 0 \\ 0 & k_T \cdot [ATP] & -k_2 - k_{-T} & 0 \\ 0 & 0 & k_2 & 0 \end{bmatrix}. \tag{s46}$$

For f|f steps the master equation is subject to the initial conditions:

$$\vec{p}(t=0) = \begin{bmatrix} 1 \\ 0 \\ 0 \\ 0 \end{bmatrix}. \tag{s47}$$

The observable dwell time distribution, $\frac{dq}{dt}$, is given by:

$$\frac{dq}{dt}(t|k_D, k_{-D}, k_T, k_{-T}, k_2) = k_2 \cdot p_3(t). \tag{s48}$$

As is, the model has five free parameters. These can be reduced to two parameters by using the measured values of $K_{f|f}$, $V_{f|f}$, and K_I, defined by the expression $K_I \equiv K_{f|f}/d$. Using the results of section s10 we showed:

$$K_{f|f} = \frac{k_2 + k_{-T}}{k_T} \cdot \frac{k_D}{k_D + k_2}, \tag{s49}$$

$$V_{f|f} = k_2 \cdot \frac{k_D}{k_D + k_2}, \tag{s50}$$

$$K_I = \frac{k_D}{k_{-D}}. \tag{s51}$$

From these expressions we solve for k_T, k_D and k_{-D} in terms of k_2, k_{-T} and the measured parameters:

$$k_D = V_{f|f} \cdot \frac{k_2}{k_2 - V_{f|f}}, \tag{s52}$$

$$k_T = \frac{k_{-T} + k_2}{K_{f|f}} \cdot \frac{V_{f|f}}{k_2}, \tag{s53}$$

$$k_{-D} = \frac{k_D}{K_I}. \tag{s54}$$

Using these expressions, the matrix M depends only on k_2 and k_{-T}. To estimate these parameters, we evaluate the log likelihood function on a two-dimensional grid spanned by guess values of k_2 and k_{-T}:

$$log(L(k_2, k_{-T}|t)) = \Sigma_{i=1}^{N} \Sigma_{j=1}^{n_i} log(\frac{dq}{dt}(t_j|k_2, k_{-T})), \tag{s55}$$

where i indexes the sum over each experimental condition and j indexes a sum over each measured data point at those conditions. We only use the ATP titration experiments at [ADP] = 0 in the likelihood analysis

and then use equation s54 to solve for k_{-D}. Figure s10 shows the result of this calculation for several DNA positions. For most DNA positions there is a clear likelihood peak around the values of k_2 and k_{-T} which maximize the likelihood function.

To estimate the errors we note that both $K_{f|f}$ and $V_{f|f}$ have measurement errors associated with their values. We repeated the calculation s55 for the log likelihood 200 separate times for each DNA position by monte carlo sampling the joint distribution of $K_{f|f}$ and $V_{f|f}$ to build the distribution of possible values of $k_{\pm T}, k_2$ and $k_{\pm D}$. For each monte carlo sample we extracted the values of k_2 and k_{-T}. For each sample of k_2 and k_{-T} we used equations s52-s54 to calculate the other model parameters (Table s7). The collection of monte carlo samples are distributions of the model parameter values. We report the mean and standard deviation of these distributions in table s6. The log likelihood at several DNA positions (6.5,13.5,23.5) did not decay at increasing k_{-T}. This may be because the distribution of dwell times (equation s55) is sensitive to k_{-T} at low $[ATP]$ (42), however much of the data was obtained at higher concentrations. More data at low $[ATP]$ would likely lead to a better resolved peak.

We examined a variant of this model, in which ATP directly induces a transition from the [ATP]-dependent step to the [ATP]-independent step (figure s10b). In the absence of ADP we can write the dwell time distribution for f|f steps as:

$$\frac{dq}{dt}(t) = \frac{V \cdot [ATP]}{[ATP] - K}(e^{-V \cdot t} - e^{-\frac{V \cdot [ATP] \cdot t}{K}}). \tag{s56}$$

This model has no free parameters. Repeating the calculation of equation s55 with the dwell time distribution s56, and evaluating the AIC for each model, we find that for Model 1 the AIC is -8868 and for the alternative model the AIC is -8671, suggesting that Model 1 better describes the data.

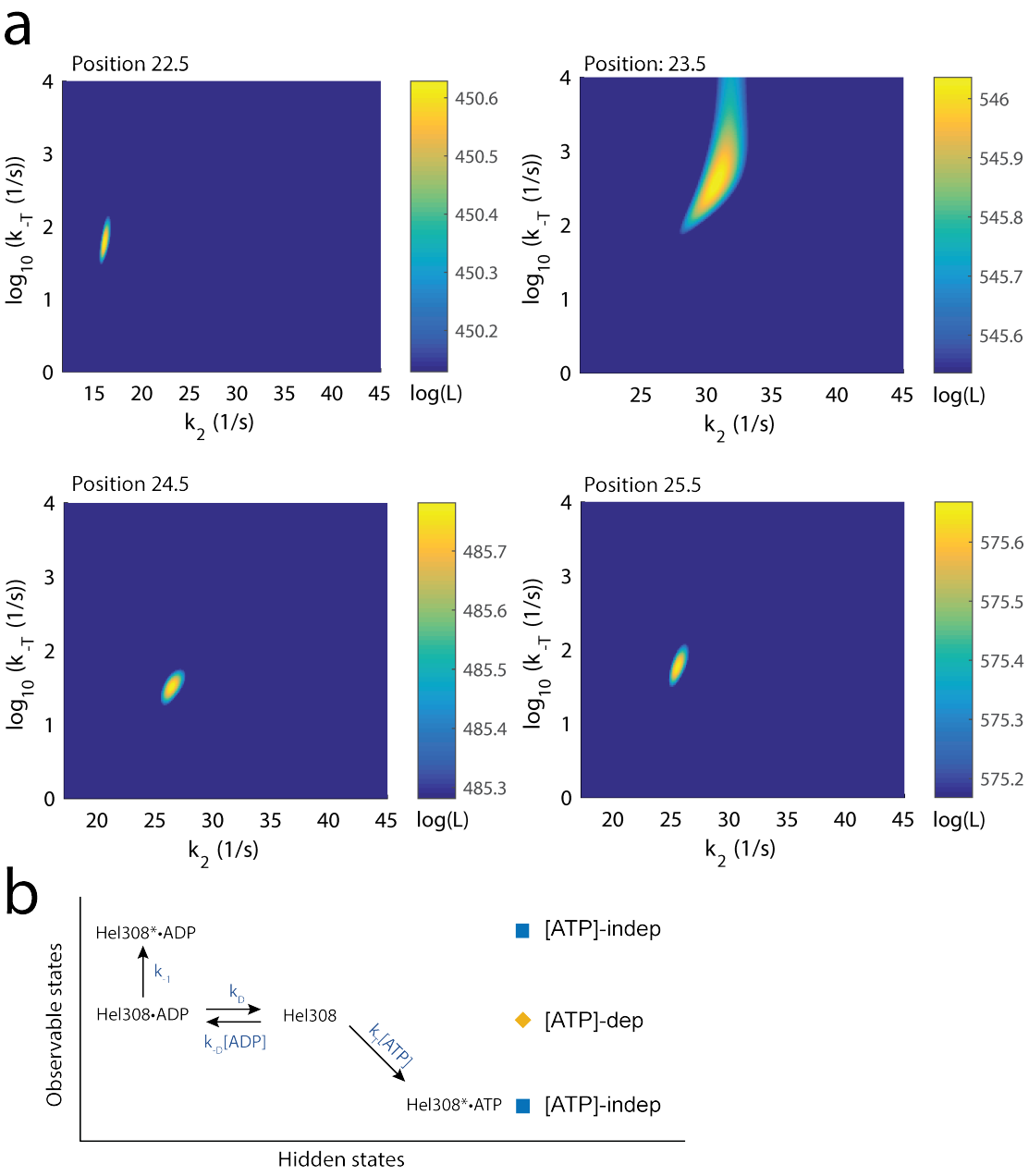

FIGURE S10. (a) Log likelihood function (equation s55) for several [ATP]-dependent steps to determine the values of the parameters k_2 and k_{-T}. The x-axis shows test values of k_2, the y-axis is the log of test values of k_{-T}, and the color axis is the log Likelihood for a single realization of the Monte-Carlo values of $K_{f|f}$ and $V_{f|f}$. The peak in yellow is evidence of a single maximum value. The log likelihood function at DNA position 23.5 did not decay with increasing k_{-T}, possibly indicating a lack of data at low $[ATP]$. (b) An alternative Model 1. Rather than binding as a hidden step, ATP directly induces the conformational change of Hel308.

DNA position (nt)	$K_{f\|f}(\mu M)$	$V_{f\|f}(s^{-1})$	$K_I(\mu M)$
0.5	82 ± 24	11.3 ± 1.5	31 ± 14
1.5	92 ± 44	10.1 ± 2.1	68 ± 48
2.5	412 ± 125	23.5 ± 3.6	81 ± 36
3.5	329 ± 40	11.0 ± 0.7	62 ± 19
4.5	181 ± 41	28.6 ± 3.2	47 ± 17
5.5	174 ± 44	12.8 ± 1.5	30 ± 9
6.5	153 ± 35	13.9 ± 1.2	30 ± 9
7.5	237 ± 67	12.4 ± 1.6	40 ± 17
8.5	100 ± 33	16.0 ± 2.3	18 ± 8
9.5	214 ± 59	23.6 ± 3.8	57 ± 25
10.5	241 ± 51	19.0 ± 1.9	65 ± 24
11.5	143 ± 55	21.0 ± 3.8	46 ± 23
12.5	110 ± 21	16.4 ± 1.3	37 ± 16
13.5	228 ± 82	22.0 ± 3.6	37 ± 17
14.5	66 ± 24	10.2 ± 1.5	49 ± 25
15.5	117 ± 51	23.4 ± 3.8	35 ± 22
17.5	75 ± 12	9.6 ± 0.7	21 ± 6
18.5	215 ± 40	34.0 ± 3.0	57 ± 13
19.5	108 ± 27	15.0 ± 1.6	37 ± 12
22.5	97 ± 18	14.7 ± 1.1	42 ± 16
23.5	250 ± 46	25.4 ± 2.5	55 ± 24
24.5	255 ± 62	23.3 ± 3.0	73 ± 26
25.5	140 ± 70	22.9 ± 4.4	40 ± 27
26.5	152 ± 26	26.4 ± 1.8	33 ± 12

TABLE S6. [ATP]-dependent step kinetic parameters as defined in section s10.

DNA position (nt)	$k_T(\mu M^{-1} \cdot s^{-1})$	$k_{-T}(s^{-1})$	$k_2(s^{-1})$	$k_D(s^{-1})$	$k_{-D}(\mu M^{-1} \cdot s^{-1})$
0.5	0.36 ± 0.04	19 ± 3	11.6 ± 1.2	179 ± 11	5.7 ± 2.4
1.5	0.56 ± 0.22	34 ± 10	9.9 ± 2.0	247 ± 54	3.8 ± 2.4
2.5	0.28 ± 0.07	99 ± 3	25.9 ± 3.4	303 ± 28	3.7 ± 1.7
3.5	0.14 ± 0.03	36 ± 3	12.2 ± 1.5	114 ± 14	1.8 ± 0.5
4.5	0.61 ± 0.08	85 ± 8	30.3 ± 2.9	410 ± 24	9.1 ± 3.4
5.5	0.28 ± 0.04	38.8 ± 2.4	13.9 ± 1.4	162 ± 12	5.3 ± 1.6
6.5*	4.4 ± 1.5	709 ± 94	15.5 ± 1.5	127 ± 5	4.3 ± 1.2
7.5	0.59 ± 0.18	125 ± 10	12.8 ± 1.9	226 ± 16	5.7 ± 2.4
8.5	0.26 ± 0.02	12 ± 2	19.1 ± 1.3	103 ± 5	5.8 ± 2.4
9.5	0.44 ± 0.03	76 ± 9	24.8 ± 2.9	323 ± 11	5.6 ± 2.4
10.5	0.27 ± 0.04	57 ± 3	22.8 ± 2.6	118 ± 5	1.8 ± 0.7
11.5	0.28 ± 0.03	22 ± 2	23.7 ± 2.1	167 ± 8	3.6 ± 1.8
12.5	0.40 ± 0.06	30 ± 2	18.4 ± 1.6	140 ± 7	3.8 ± 1.6
13.5*	0.87 ± 0.28	184 ± 33	23.9 ± 2.9	265 ± 12	7.0 ± 3.1
14.5	0.39 ± 0.06	17 ± 2	11.1 ± 1.0	119 ± 9	2.4 ± 1.2
15.5	0.30 ± 0.05	12 ± 2	26.2 ± 2.0	274 ± 30	7.8 ± 4.8
17.5	0.29 ± 0.03	13 ± 2	10.6 ± 1.2	103 ± 5	5.0 ± 1.5
18.5	0.30 ± 0.04	35 ± 2	38.7 ± 3.3	240 ± 27	4.2 ± 0.8
19.5	0.38 ± 0.07	30 ± 2	18.0 ± 1.5	118 ± 5	3.2 ± 1.0
22.5	0.69 ± 0.11	58 ± 4	16.2 ± 1.4	172 ± 8	4.1 ± 1.5
23.5*	1.26 ± 0.12	346 ± 45	30.6 ± 2.9	189 ± 8	3.5 ± 1.6
24.5	0.21 ± 0.02	30 ± 3	24.9 ± 2.7	228 ± 9	3.1 ± 1.1
25.5	0.56 ± 0.08	56 ± 6	24.0 ± 2.2	370 ± 20	9.3 ± 6.2
26.5	0.46 ± 0.06	51 ± 4	31.0 ± 2.3	181 ± 9	5.4 ± 1.9

TABLE S7. [ATP]-dependent step kinetic parameters as in figure s8, calculated from equation s55. The likelihood function for those steps with an asterisk next to them did not decay as $k_{-T} \to \infty$, suggesting that the values of k_{-T} and k_T cannot be trusted.

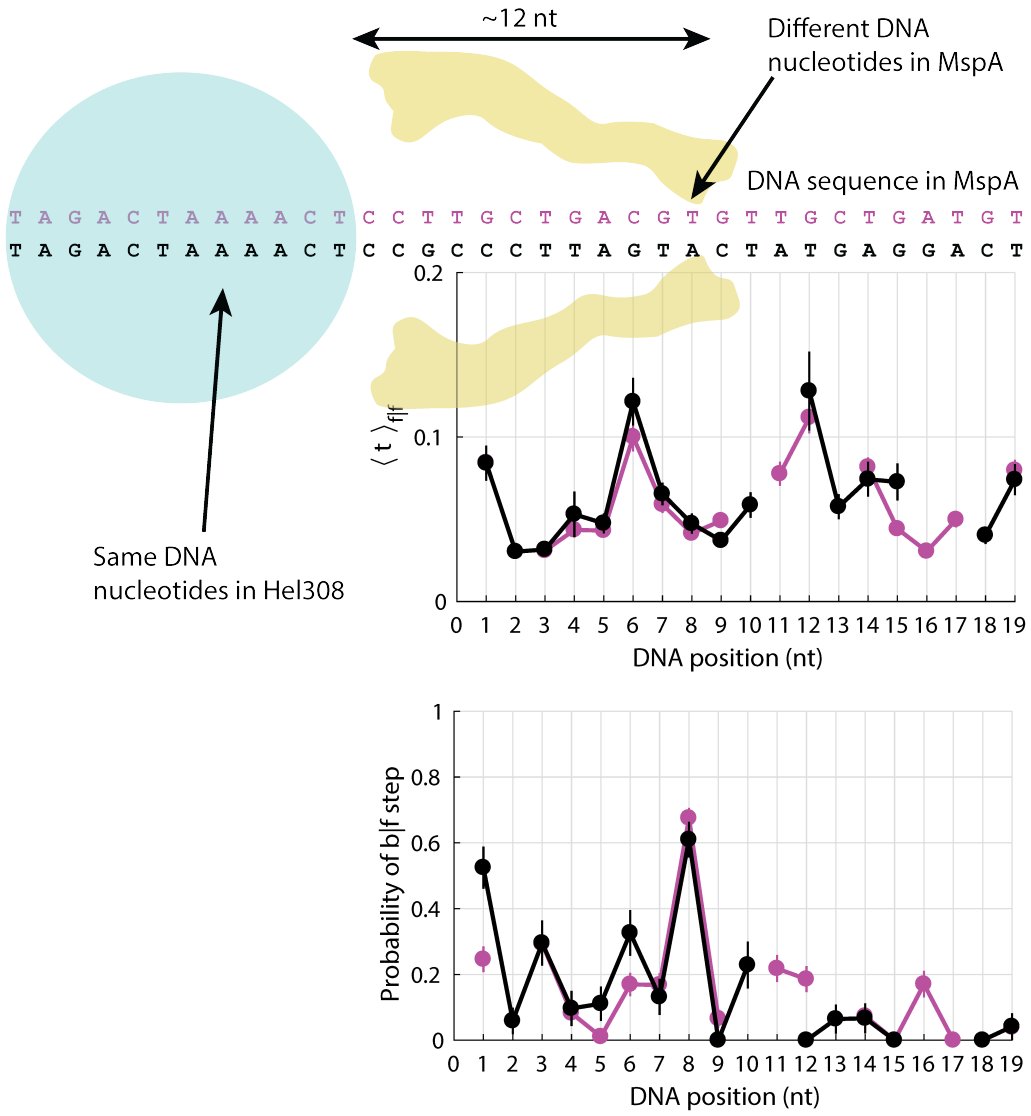

FIGURE S11. (top) The average dwell time of $f|f$ [ATP]-independent steps vs DNA position for two DNA sequences. The DNA sequence in the MspA pore is indicated above. An illustration of the experimental scheme indicating that the DNA nucleotides in Hel308 are the same while the nucleotides in MspA are different. Gaps indicate positions where the measurement could not be made due to degeneracy of the ion-current signal. Measurements were taken at elevated temperature of 37 °C to increase the rate of DNA entry into the nanopore. (bottom) Probability of a $b|f$ [ATP]-independent step vs DNA position for two DNA sequences.

13. Materials and Methods

- **Pore establishment**: A single M2-NNN MspA nanopore was established in a 1,2-diphytanoyl-sn-glycerol-3-phosphocholine (dphpc) or a (dopc) lipid bilayer using methods that have been well established (26). Lipids were ordered from Avanti Polar Lipids.
- **DNA preparation**: A complementary DNA strand was annealed to the template DNA strand so that the template has a free 5′ end, and an 8-base 3′ overhang. Hel308 binds to this overhang, and can begin to unwind dsDNA in solution, meaning that an event can start at any location along the DNA molecule. To prevent accumulation of ADP in bulk we perfused new reagents every 45 minutes.

The 5′ end of the template is drawn into the pore, dissociating the complement. If a Hel308 is bound to the DNA it will translocate from 3′ to 5′, drawing the ssDNA out of the pore. While in principle it is possible for DNA to go through the pore in the 3′ orientation, no such events were observed.

The DNA sequence for the template strand is:

5′ PTACTACTACTACTACTACXXTTTTTCAGGAGTATCATGATTCCCGCCTCAAAATCA-GATCTCACTATCGCATTCTCATGCAGGTCGTAGCC 3′

The DNA sequence for the complementary strand is:

5′ CCTGCATGAGAATGCGATAGTGAGATTTTTTTTTTTTTTTTTTTZ 3′.

P is a phosphate group to facilitate insertion of the 5′ end of the DNA into the nanopore, X is an abasic, and Z is a cholesterol tag to localize the DNA to the bilayer and increase the rate of DNA capture by the pore. DNA was ordered from PAN Protein and Nucleic Acid facility at Stanford. DNA was annealed by mixing template and complement strands at a 1.2:1 molar ratio, denaturing at 95 °C for 3 minutes, and then cooling to 4 °C over 10 minutes.

- **Proteins**: Hel308 from Thermococcus gammatolerans EJ3 (accession number WP_015858487.1) and M2-NNN MspA (accession number CAB56052.1) were prepared as described previously(27).
- **Operating conditions**: All experiments were run at 400 mM KCl, with 10 mM HEPES at pH 8.0 and 10 mM MgCl2. Once a single M2-NNN MspA nanopore was established, a buffer with the above conditions along with ATP and ADP at concentrations described in the supplement was perfused to the cis well. ATP and ADP were ordered from Sigma Aldrich. The perfusion is done to maintain constant concentrations in the reaction volume. DNA, DTT, and Hel308 were added to final concentrations of 5 nM, 1 mM, and 50 nM, respectively.

  For measurements at elevated temperature, a Thorlabs temperature controller (2A/12W TEC 2000 B2) powered a Peltier element placed in thermal contact with a large copper plate and an aluminum holder for the Teflon cell. Temperature measurements were made with a calibrated OMEGA precision thermistor 44008. The thermistor was inserted into a third well cell identical to the cis well, filled with buffer, centered on the Teflon cell.
- **Data acquisition**: Data was acquired on an Axopatch 200B amplifier at 50 kHz, and downsampled by averaging to 5 kHz.
- **Data sharing**: Data and code is available through figshare.

14. References

(26) Laszlo, Andrew H., Ian M. Derrington, and Jens H. Gundlach. “MspA nanopore as a single-molecule tool: From sequencing to SPRNT.” Methods 105 (2016): 75-89.

(27) Derrington, Ian M., et al. “Subangstrom single-molecule measurements of motor proteins using a nanopore.” Nature biotechnology 33.10 (2015): 1073-1075.

(28) Laszlo, Andrew H., et al. “Decoding long nanopore sequencing reads of natural DNA.” Nature biotechnology 32.8 (2014): 829-833.

(29) Manrao, Elizabeth A., et al. “Reading DNA at single-nucleotide resolution with a mutant MspA nanopore and phi29 DNA polymerase.” Nature biotechnology 30.4 (2012): 349-353.

(30) Tsygankov, Denis, Martin Lindn, and Michael E. Fisher. “Back-stepping, hidden substeps, and conditional dwell times in molecular motors.” Physical Review E 75.2 (2007): 021909. APA

(31) Chemla, Yann R., Jeffrey R. Moffitt, and Carlos Bustamante. “Exact solutions for kinetic models of macromolecular dynamics.” The Journal of Physical Chemistry B 112.19 (2008): 6025-6044.

(32) Keller, David, and Carlos Bustamante. “The mechanochemistry of molecular motors.” Biophysical Journal 78.2 (2000): 541-556.

(37) Needleman, Saul B., and Christian D. Wunsch. “A general method applicable to the search for similarities in the amino acid sequence of two proteins.” Journal of molecular biology 48.3 (1970): 443-453.

(38) Durbin, Richard, et al. Biological sequence analysis: probabilistic models of proteins and nucleic acids. Cambridge university press, 1998.

(39) Hurvich, Clifford M., and Chih-Ling Tsai. “Regression and time series model selection in small samples.” Biometrika (1989): 297-307.

(40) Barrio, Manuel, Andr Leier, and Tatiana T. Marquez-Lago. “Reduction of chemical reaction networks through delay distributions.” The Journal of chemical physics 138.10 (2013): 104114.

(41) Qian, Hong, and Elliot L. Elson. "Single-molecule enzymology: stochastic MichaelisMenten kinetics." Biophysical chemistry 101 (2002): 565-576.

(42) Kou, S. C., et al. "Single-molecule michaelis menten equations." (2005): 19068-19081.

(43) Boas, Mary L. Mathematical methods in the physical sciences. Vol. 2. New York: Wiley, 1966.

(44) Walcott, Sam. "The load dependence of rate constants." The Journal of chemical physics 128.21 (2008): 06B601.